Spectrochimica Acta Part A: Molecular and Biomolecular Spectroscopy 270 (2022) 120754

Contents lists available at ScienceDirect

Spectrochimica Acta Part A: Molecular and Biomolecular Spectroscopy

journal homepage: www.elsevier.com/locate/saa

High resolution spectroscopic measurement of $^{130}Te_2$: Reference lines near 444.4 nm for *e*EDM experiment using PbF molecules

Qinning Lin [a], Renjun Pang [a], Zesen Wang [a], Shunyong Hou [a], Hailing Wang [a], Jianping Yin [a,*], Tao Yang [a,b,*]

[a] State Key Laboratory of Precision Spectroscopy, East China Normal University, Shanghai 200062, PR China
[b] Collaborative Innovation Center of Extreme Optics, Shanxi University, Taiyuan, Shanxi 030006, PR China

HIGHLIGHTS

- 187 electronic transition lines for $^{130}Te_2$ over the range of 400 GHz were presented with a frequency uncertainty of 62 MHz;
- $B_1(^3\sum_u^-)0_u^+(\upsilon' = 10) \leftarrow X_1(^3\Sigma_g^-)0_g^+(\upsilon = 5)$ transitions were identified while the Dunham parametersT_υ,B_υ,D_υ andH_υ of the B_1 $(\upsilon' = 10)$ state were updated;
- Exploring reference lines for further PbF *e*EDM spectroscopic measurement.

GRAPHICAL ABSTRACT

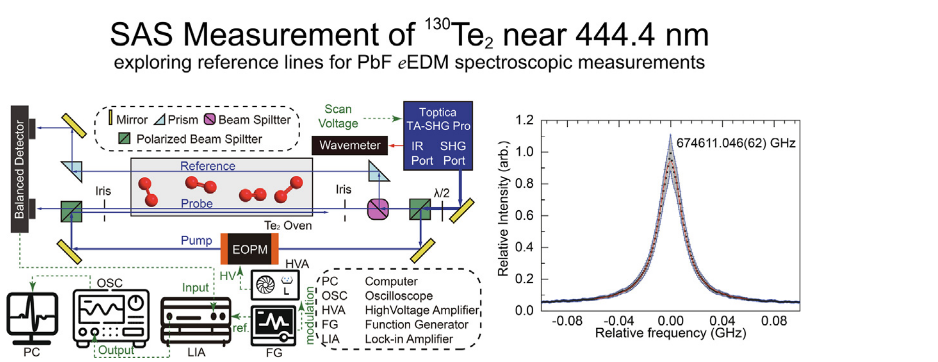

ARTICLE INFO

Article history:
Received 4 September 2021
Received in revised form 8 December 2021
Accepted 10 December 2021
Available online 14 December 2021

Keywords:
Tellurium spectrum
Saturated Absorption Spectroscopy
Frequency reference
electron's Electric Dipole Moment (*e*EDM)

ABSTRACT

Molecular tellurium (Te_2) offers a wide range of potential applications, including frequency reference. Spectroscopic results about the $^{130}Te_2$ spectrum were previously reported, but few lines lie around the PbF transition of A $(^2\Sigma^+)$ $(\upsilon' = 0) \leftarrow X_1^2\Pi_{1/2}$ $(\upsilon = 0)$ (~444.4 nm) which is regarded as an *e*EDM (electron's Electric Dipole Moment) sensitive transition. Here electronic transition lines for $^{130}Te_2$ were determined using the Saturated Absorption Spectroscopy method, where the origin of the transition band was investigated for the B_1 $(^3\Sigma_u^-)0_u^+$ $(\upsilon' = 10) \leftarrow X_1$ $(^3\Sigma_g^-)0_g^+$ $(\upsilon = 5)$ transition. The Dunham model with high orders was utilized to assign these transition lines, while Dunham parameters of the excited state B_1 $(\upsilon' = 10)$ were updated to a new level. The Toptica TA-SHG Pro laser was then locked to a single absorption line using a P-I servo. Our results here not only provide the assigned atlas of Te_2 spectrum near 444.4 nm, but also contribute to a stable and sensitive spectroscopic detection of PbF molecules toward the *e*EDM measurement, which is significant in understanding the fundamental physics beyond the Standard Model.

1. Introduction

The measurement of the electron's Electric Dipole Moment (*e*EDM) has been a state-of-the-art technique in search of new physics beyond the Standard Model. Though only a few experimental results have been obtained upon molecules such as YbF [1], HfF^+ [2] and ThO [3], these still cannot confirm the existence of an non-zero *e*EDM value. There are still more tentative molecular

* Corresponding authors at: State Key Laboratory of Precision Spectroscopy, East China Normal University, Shanghai 200062, PR China (T. Yang).
E-mail addresses: jpyin@phy.ecnu.edu.cn (J. Yin), tyang@lps.ecnu.edu.cn (T. Yang).

https://doi.org/10.1016/j.saa.2021.120754
1386-1425/

systems, such as RaF [4], RaH [5], BaF [6], HgF [7], HgBr [8], BaOH [9], WC [10], YbOH [11], and PbF [12,13], have been investigated for their suitability for an *e*EDM measurement. As a diatomic molecule, PbF possesses numerous properties that are beneficial to measuring *e*EDM, including the large dipole moment, strong internal electric field and small sensitivity to external magnetic field [14,15]. In the proposed *e*EDM measurement, PbF molecules carrying the *e*EDM phase can be detected via spectroscopic methods such as the resonance-enhanced multiphoton ionization through the A (υ' = 0, J = 1/2, F = 1, M_F = 0) ← X_1 (υ = 0, J = 1/2, F = 1, $|M_F|$ = 1) transition of about 444.4 nm [14]. It is therefore crucial to have reference lines around the required transition [15] for stabilizing the laser system, eliminating the long term frequency drift (1 GHz/hour) of narrow-linewidth laser due to mechanical or thermal destabilization.

Atomic or molecular absorption lines are effective absolute frequency standards for optical lasers, since they can cover a specific range of wavelengths while maintaining a high level of stability. The molecular tellurium absorption band covers the range between 350 nm and 600 nm [16 17], and the most complete absorption spectrum has been characterized by J. Cariou and P. Luc from 420 nm to 540 nm[18]. In the 1980 s, dye lasers were utilized to conduct supplementary work [19], in order to update the spectroscopic constants of its ground and excited states [20–22]. Saturated Absorption Spectroscopy (SAS) or Modulation Transfer Spectroscopy (MTS) were extensively conducted in recent years on the Te_2 spectrum as frequency standards in the 400–600 nm range [23–29]. However, there are only 11 lines reported in our desired range of 444.4 ± 0.05 nm [26], which are not sufficient to address the molecular transitions of PbF A (υ' = 0, J = 1/2) ← X_1 (υ = 0, J = 1/2) even by the aid of acousto-optic modulators (AOMs) or electric-optic modulators (EOMs).

Therefore, it is vital to measure more specific molecular Te_2 transition lines that lie around PbF A (υ' = 0, J = 1/2) ← X_1(υ = 0, J = 1/2), which are crucial to carry out the sensitive spectroscopic detection of PbF molecules in an *e*EDM experiment. Here, we demonstrate the optical scanning results of Te_2 lines around 674600 GHz by a SAS method, which present 187 lines across a frequency range of roughly 400 GHz with the linewidth closed to the natural one. These molecular transitions are further analyzed using the Dunham model and the least squares fitting method, in order to shed more lights on the Dunham parameters T_υ,B_υ,D_υ and H_υ of B_1 state (υ' = 10) in a significant level. The frequency of a Toptica TA-SHG Pro laser may be stabilized with greater than 10 MHz accuracy (10^{-8} $\Delta f/f$) by locking to a single absorption line via a P-I servo. Our results not only provide the detailed frequency reference atlas near 444.4 nm which can be extended to other spectral range of Te_2, but also contribute to a stable and sensitive spectroscopic measurement of PbF in an *e*EDM experiment that is insightful for understanding parity and time-reversal violating effects in the fundamental physics.

2. Experimental details

Fig. 1 illustrates the experimental setup of the Saturated Absorption Spectroscopy using a Te_2 cell. The isotopic $^{130}Te_2$ was uniformly heated in a cylindrical glass cell (purity greater than 99.3 %; Opthos instruments, Part No. AC-T) maintained at 600 °C where the tellurium vapor pressure is around 1 Torr. With two counter-propagating laser beams and a reference beam, the absorption spectrum of Te_2 were studied using the SAS method. The "pump" beam (reflected) and another transmitted light were created by dividing the original beam from the blue laser (Toptica, TA SHG-Pro) through a polarizing beam splitter (PBS, Thorlabs, PBS101), allowing the splitting ratio between them to be changed using a λ/2 wave plate (Newport, 05RP12-10). The transmitted beam was then split into two parts using an unpolarized beam splitter (Lbtek, BS1055-A): the probe beam, which was directly transmitted through the cube and into the Te_2 oven, and the reflected beam, which was parallel with the probe beam after a 90° prism mirror (Lbtek, RAP105-A) for reference. The pump beam went through the Te_2 cell after another PBS, sharing the same beam path as the probe laser but in the opposite direction, after being reflected by two mirrors (CVI Optics, TLM1-450–45-4050). The pump beam was held at 50 mW to saturate the Te_2 absorption, while the probe and reference beams were kept around 50 μW. A balanced Si Photodetector (Thorlabs, PDB210A) was used to receive the absorption signal, which can produce an output signal proportionate to the intensity difference between the probe and reference beams.

A ramp scanning voltage (0.05 V_{pp}, 1 Hz) was created by a function generator (HP, 3245A) and then applied to the Toptica laser diode's piezo voltage, resulting in a scan range of 0.5 GHz, and the entire scan was performed piece by piece with a 0.1 GHz overlap. Frequency may also be shifted by changing the voltage offset of the PZT, allowing it to be tuned beyond 30 GHz in IR without mode hop. The PZT scan has a scanning error basically due to the unstable applied voltage [26] while it is small enough to neglect. The fundamental wavelength (IR, 888.8 nm) of laser was monitored by a wavemeter (Highfineness, WSU-30) whose calibration will be described later. The pump beam was modulated at 200 Hz with an EOPM (Thorlabs, EO-PM-NR-C4). The signal from the photodetector output was demodulated using a Lock-in amplifier (EG&G, Model 5210), and the signal was then collected using an oscilloscope (Tektronix, DPO4104B) and transferred to a computer.

3. Experimental results

Within twelve hours, the SAS technique detected 187 lines ranging from 674387 to 674797 GHz. Table 1 summarizes the observed transition lines, and Fig. 2 illustrates the resulting spectrum. The line 101 corresponds to line [1525] in the tellurium atlas [18] and the relative intensities are normalized with respect to the line 101. A typical transition was also presented in the inset of Fig. 2 where the waveform collected by an oscilloscope is shown as black squares. The red solid line agrees with a Lorentz fit with a reduced R^2 value greater than 0.9984 and a FWHM of 22.40(4) MHz.

In our experiment, the uncertainty for the frequency measurement basically attributes to the short-term instability of the laser frequency, the wavemeter's long-term drift and the wavemeter's absolute accuracy. The short-term uncertainty has been evaluated by measuring the line 101 for 500 times, providing an uncertainty of 6.36 MHz (95% confidence interval). The long-term uncertainty during the whole experiment (12 h) is ∼ 3 MHz according to wavemeter's specifications and Ref. [30]. The absolute uncertainty is considered to be the absolute accuracy of the wavemeter itself (30 MHz). Since the wavemeter measures the fundamental wavelength (∼888.8 nm) during the whole experiment and the SHG output (444.4 nm) has been sent to the Tellurium cell for scanning, the combined uncertainty is doubled to be about 62 MHz for the entire spectrum. The uncertainty of intensity has also been evaluated, which indicates a standard deviation of 0.029, leading to the statistical uncertainty of 5.8 % (Fig. 2).

4. Discussion

4.1. Calibration of wavemeter

During the experiment, a difference of approximately ∼ 4 GHz gap (∼2 GHz in IR) was discovered between the wavemeter read-

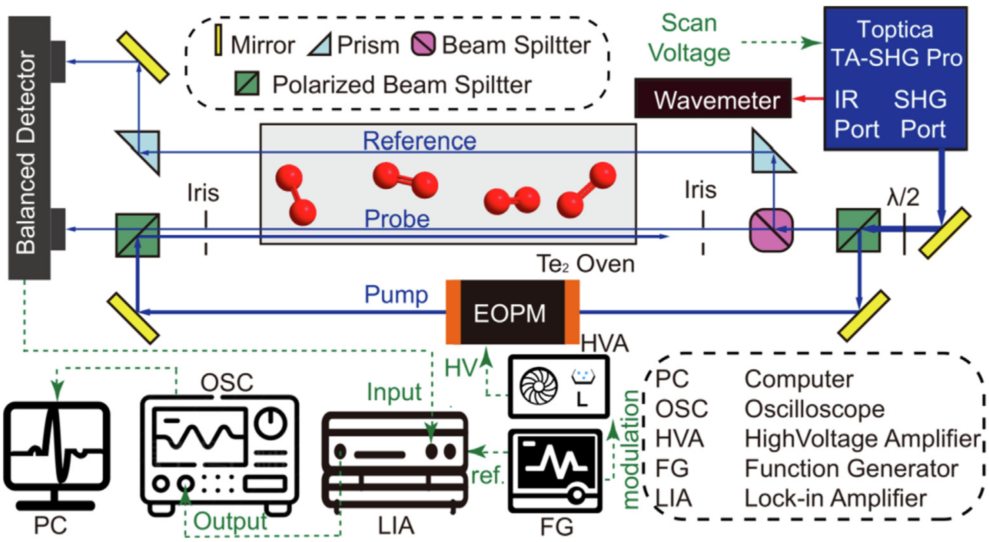

Fig. 1. Experimental setup for the SAS spectroscopy surrounding the tellurium cell (Not to scale). Red: fundamental laser output (~888.8 nm); blue: SHG laser output (~444.4 nm); green dashed: electrical signal. (For interpretation of the references to colour in this figure legend, the reader is referred to the web version of this article.)

outs and the known transition frequencies published by Cariou *et al.* [18] It is worth noting that the fundamental laser from the IR port (~888.8 nm) has been sent to the wavemeter (HighFinesse WSU-30) for frequency readout (Fig. 1). A similar SAS method was utilized to address the calibration by adopting a cesium cell at the room temperature. The initial beam from the Toptica laser's IR Port (~895 nm) was split through a polarizing beam splitter (Thorlabs, PBS102), allowing most of the light reflected to be transmitted as the pump beam went across the Cs cell. Then the pump beam went through a λ/4 wave plate (Newport, 10RP04-31) and a round continuously variable ND filter (Daheng optics, GCO-0704 M). After being reflected by a mirror (Thorlabs, PF10-01-P01), the probe beam went through the cell in the opposite direction along the same beam path and was transmitted via the PBS. The pump beam was held at 20 mW and the probe beam was kept around 50 μW, which can be adjusted by rotating the ND filter. A Si Switchable Gain Detector (Thorlabs, PDA36A2) was used to receive the absorption signal, which was then captured by the same oscilloscope.

Udem *et al.* [31] measured the Cesium D_1 line using a mode-locked laser, obtaining the absolute optical frequency of four hyperfine transitions between $F = 4$ and $F = 3$ states. Table 2 summarizes frequency readouts from the wavemeter and measurements of those transition lines. The $F_g = 4 \rightarrow F_e = 3$ transition was measured 500 times, yielding an average readout value of 335109.396 GHz, suggesting that the difference between the wavemeter's readout and actual frequency should be 1.974 GHz. Unless otherwise specified, all frequencies in this work were calibrated with respect to this difference.

4.2. Comparison with previous results

Here, 22 lines are identified by comparing them with the known Te_2 lines of the Cariou's atlas [18], whose measured frequencies are in good agreement with the previous data within 40 MHz. The result was then summarized in Table 3.

4.3. Line assignment for X_1-B_1 transition

Previous work computed the Dunham parameters for the A and B_1 states of $^{130}Te_2$ [21]. The band origin of B_1 $(^3\Sigma_u^-)0_u^+$ (υ' = 10) ← $X_1(^3\Sigma_g^-)0_g^+$ (υ = 5) transition was discovered to be about 674700 GHz and the low rotational (up to $J = 40$) spectrum was covered by this scanning range. Only P and R branches appear in this spectrum while the Q branch is forbidden since $\Omega = 0$ [32]. Therefore, the assignment for this transition was performed for P and R branches only.

The Dunham model [33] was applied to our scanning result to determine the frequency of a specific transition and the brief explanation is presented here. Diatomic molecules have two degrees of freedom, namely vibration and nuclei rotation with respect to one another. The vibration of two nuclei can be regarded as a quantum harmonic oscillator with the energy level form like $E_\upsilon = \hbar\omega(\upsilon + 1/2)$ where υ is the vibrational quantum number and the rotational energy can be calculated with the quantum angular momentum operator yielding energy levels $E_J = (\hbar^2/2I)J(J+1)$, where J is the rotational quantum number. When rotation and vibration occur simultaneously, a model with higher order coupling terms is employed to explain the ro-vibrational energy level, which may be characterized by Dunham parameters as in Eq. (4.1), where T_υ and B_υ denote the electronic energy and rotational constant respectively, and D_υ and H_υ represent the centrifugal distortion constants.

$$E_{\upsilon J} = T_\upsilon + B_\upsilon J(J+1) + D_\upsilon (J(J+1))^2 + H_\upsilon (J(J+1))^3 + \cdots \quad (4.1)$$

Despite the fact that 187 lines were discovered during the scan, only a handful of them are related to this transition, indicating that a new approach must be used to identify B_1 $(^3\Sigma_u^-)0_u^+$ (υ' = 10) ← $X_1(^3\Sigma_g^-)0_g^+$ (υ = 5) transition lines from others before the assigning operation. Previous published values were obtained from Ref. [21] and parameters can be adjusted by making corrections to them. The best-fit parameters are assumed to be able to match the majority of the lines.

The parameters of the ground state were treated as invariants, whereas the values of T_υ and B_υ of excited state $B_1(\upsilon' = 10)$ were initially considered. A tiny frequency range was applied to the previously reported value, which was then split into a grid. If there is at least one experimental transition line within the tolerance range, it will be considered as matched with the computed result. The matching procedure was repeated until all of T_υ and B_υ sets were completed, in which the one corresponding to most of the matched lines was discovered.

Since all of the transition lines have been identified, the assigning method may be performed using the least squares polynomial

Table 1
SAS lines of tellurium near 444.4 nm (relative frequency and intensity are given with respect to the line 101). Numbers in parentheses indicate the overall uncertainty in the last two digits.

No.	Freq. (GHz)	Rel. freq. (GHz)	Rel. Int.	No.	Freq. (GHz)	Rel. freq. (GHz)	Rel. Int.
1	674387.814(62)	−223.233	4.10	96	674602.230(62)	−8.817	0.79
2	674389.902(62)	−221.145	3.53	97	674606.131(62)	−4.916	3.10
3	674390.373(62)	−220.674	0.28	98	674607.674(62)	−3.372	5.30
4	674394.159(62)	−216.887	4.33	99	674609.765(62)	−1.281	1.02
5	674402.204(62)	−208.842	0.37	100	674610.750(62)	−0.297	0.53
6	674403.066(62)	−207.980	0.90	101	674611.046(62)	0.000	1.00
7	674405.899(62)	−205.148	1.07	102	674611.656(62)	0.609	0.73
8	674406.311(62)	−204.735	1.64	103	674613.634(62)	2.588	2.85
9	674406.624(62)	−204.423	0.44	104	674613.811(62)	2.765	0.15
10	674407.379(62)	−203.667	1.02	105	674615.355(62)	4.308	4.98
11	674409.665(62)	−201.381	3.57	106	674616.009(62)	4.963	3.06
12	674411.033(62)	−200.013	1.98	107	674623.314(62)	12.267	0.13
13	674414.794(62)	−196.252	2.65	108	674623.471(62)	12.425	1.84
14	674419.400(62)	−191.646	1.23	109	674623.692(62)	12.645	0.16
15	674420.773(62)	−190.274	1.36	110	674626.825(62)	15.779	0.37
16	674423.315(62)	−187.732	0.54	111	674627.320(62)	16.274	1.21
17	674428.439(62)	−182.607	3.19	112	674629.822(62)	18.775	5.38
18	674431.046(62)	−180.001	1.63	113	674629.873(62)	18.826	1.46
19	674431.543(62)	−179.504	1.48	114	674632.543(62)	21.497	3.75
20	674431.640(62)	−179.406	0.97	115	674634.981(62)	23.934	0.18
21	674447.883(62)	−163.163	2.08	116	674637.826(62)	26.780	3.00
22	674449.499(62)	−161.547	0.63	117	674641.022(62)	29.976	0.92
23	674450.042(62)	−161.005	0.46	118	674645.035(62)	33.989	2.67
24	674453.056(62)	−157.990	0.74	119	674645.334(62)	34.287	0.36
25	674453.858(62)	−157.189	1.19	120	674645.359(62)	34.313	0.59
26	674455.378(62)	−155.669	2.87	121	674646.076(62)	35.030	2.15
27	674457.270(62)	−153.776	0.82	122	674646.905(62)	35.859	3.89
28	674458.691(62)	−152.356	0.46	123	674647.227(62)	36.181	2.64
29	674460.772(62)	−150.275	3.13	124	674649.317(62)	38.271	2.50
30	674462.546(62)	−148.500	0.84	125	674656.200(62)	45.153	1.03
31	674466.404(62)	−144.642	0.72	126	674659.912(62)	48.866	0.73
32	674470.887(62)	−140.160	0.26	127	674660.636(62)	49.589	0.59
33	674475.016(62)	−136.031	0.42	128	674660.853(62)	49.806	0.81
34	674478.474(62)	−132.572	0.45	129	674662.075(62)	51.029	2.47
35	674480.954(62)	−130.093	2.41	130	674662.575(62)	51.529	2.96
36	674486.927(62)	−124.119	1.18	131	674664.175(62)	53.129	2.42
37	674487.427(62)	−123.619	0.56	132	674667.589(62)	56.543	0.75
38	674488.245(62)	−122.802	1.32	133	674668.250(62)	57.204	0.15
39	674489.592(62)	−121.454	0.22	134	674670.281(62)	59.235	1.02
40	674489.631(62)	−121.416	1.61	135	674670.706(62)	59.660	1.76
41	674491.134(62)	−119.913	4.22	136	674671.480(62)	60.434	1.36
42	674492.665(62)	−118.381	0.28	137	674674.161(62)	63.115	5.03
43	674495.947(62)	−115.099	4.15	138	674675.269(62)	64.222	4.29
44	674500.209(62)	−110.838	1.42	139	674677.067(62)	66.020	3.12
45	674503.748(62)	−107.298	0.58	140	674681.147(62)	70.101	2.15
46	674505.318(62)	−105.729	3.71	141	674682.007(62)	70.960	6.09
47	674509.205(62)	−101.841	4.18	142	674683.007(62)	71.961	1.28
48	674509.648(62)	−101.398	1.21	143	674686.517(62)	75.471	1.07
49	674510.401(62)	−100.645	0.64	144	674686.703(62)	75.657	4.88
50	674512.285(62)	−98.762	0.84	145	674687.777(62)	76.731	1.30
51	674515.010(62)	−96.037	4.49	146	674687.820(62)	76.774	1.12
52	674515.012(62)	−96.034	3.95	147	674687.901(62)	76.855	0.13
53	674516.392(62)	−94.654	0.41	148	674688.005(62)	76.959	1.49
54	674516.688(62)	−94.358	3.14	149	674688.141(62)	77.095	0.27
55	674519.576(62)	−91.471	1.26	150	674688.243(62)	77.196	0.37
56	674519.997(62)	−91.049	5.16	151	674688.285(62)	77.238	0.61
57	674520.004(62)	−91.042	2.41	152	674690.114(62)	79.067	6.76
58	674527.718(62)	−83.328	1.02	153	674695.846(62)	84.800	3.59
59	674527.822(62)	−83.224	1.94	154	674696.217(62)	85.171	1.67
60	674528.918(62)	−82.128	0.28	155	674697.067(62)	86.021	1.07
61	674530.229(62)	−80.818	0.18	156	674697.432(62)	86.385	0.87
62	674530.537(62)	−80.510	0.53	157	674698.423(62)	87.377	2.39
63	674531.656(62)	−79.390	6.10	158	674703.234(62)	92.188	2.79
64	674533.407(62)	−77.639	0.94	159	674704.140(62)	93.094	0.44
65	674539.329(62)	−71.717	3.05	160	674708.916(62)	97.870	1.30
66	674539.890(62)	−71.156	0.61	161	674711.508(62)	100.461	5.12
67	674541.052(62)	−69.995	0.96	162	674712.207(62)	101.160	0.29
68	674541.888(62)	−69.159	3.49	163	674712.713(62)	101.666	0.79
69	674545.275(62)	−65.772	3.57	164	674713.457(62)	102.411	0.47
70	674546.037(62)	−65.010	2.11	165	674713.458(62)	102.411	0.59
71	674551.252(62)	−59.795	0.83	166	674713.770(62)	102.723	1.06
72	674552.316(62)	−58.730	0.72	167	674713.790(62)	102.743	1.31
73	674555.255(62)	−55.791	2.18	168	674713.812(62)	102.766	1.22

Table 1 (*continued*)

No.	Freq. (GHz)	Rel. freq. (GHz)	Rel. Int.	No.	Freq. (GHz)	Rel. freq. (GHz)	Rel. Int.
74	674563.112(62)	−47.934	0.89	169	674713.813(62)	102.766	0.77
75	674563.809(62)	−47.237	1.24	170	674720.022(62)	108.976	0.15
76	674566.815(62)	−44.231	2.95	171	674721.015(62)	109.969	0.24
77	674567.165(62)	−43.881	2.12	172	674722.539(62)	111.493	0.73
78	674567.914(62)	−43.132	1.04	173	674724.128(62)	113.082	0.38
79	674570.570(62)	−40.477	5.07	174	674726.881(62)	115.835	0.41
80	674570.680(62)	−40.366	0.13	175	674728.495(62)	117.449	0.31
81	674573.262(62)	−37.784	2.37	176	674732.734(62)	121.688	0.19
82	674576.506(62)	−34.540	1.37	177	674734.505(62)	123.458	0.29
83	674583.196(62)	−27.850	3.42	178	674735.564(62)	124.518	0.15
84	674586.547(62)	−24.500	3.29	179	674736.571(62)	125.525	0.26
85	674588.986(62)	−22.060	4.59	180	674738.732(62)	127.686	1.18
86	674589.741(62)	−21.306	4.50	181	674742.835(62)	131.789	0.49
87	674593.148(62)	−17.898	2.61	182	674759.284(62)	148.238	0.37
88	674593.702(62)	−17.344	0.88	183	674759.453(62)	148.406	0.32
89	674595.218(62)	−15.829	4.30	184	674761.710(62)	150.664	0.29
90	674595.859(62)	−15.187	4.05	185	674765.601(62)	154.555	0.33
91	674597.829(62)	−13.218	1.38	186	674775.624(62)	164.577	0.21
92	674600.379(62)	−10.668	1.77	187	674797.074(62)	186.028	0.25
93	674602.023(62)	−9.023	1.37				
94	674602.025(62)	−9.021	1.63				
95	674602.147(62)	−8.900	0.33				

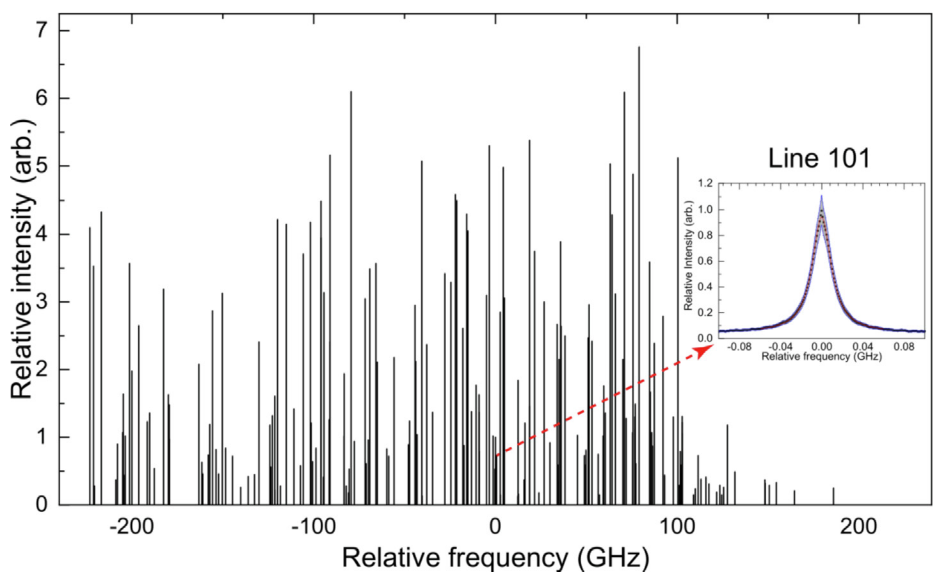

Fig. 2. Overall Spectrum near 444.4 nm obtained from the SAS method. The inset illustrates the transition line 101 (674611.046 GHz) fitted with the Lorentz profile, and frequencies of other lines are indicated with respect to the line 101. Black square: the scanning result; gray area: 95% confidence interval which are surrounded by blue solid lines; red solid line: Lorentz fit. (For interpretation of the references to colour in this figure legend, the reader is referred to the web version of this article.)

Table 2
Comparison of absolute frequencies of Cs D_1 line and wavemeter readouts.

Transition	This Work		Udem[31]		Difference (GHz)
	Frequency (GHz)	Gap (GHz)	Frequency (GHz)	Gap (GHz)	
$F_{g=3} \rightarrow F_{e=4}$	335119.758	–	335121.7305	–	1.972526
$F_{g=3} \rightarrow F_{e=3}$	335118.589	1.169	335120.5628	1.167688	1.973838
$F_{g=4} \rightarrow F_{e=4}$	335110.565	8.024	335112.5379	8.024944	1.972894
$F_{g=4} \rightarrow F_{e=3}$	335109.395	1.170	335111.3702	1.167688	1.975206

fitting to obtain the values of T_υ, B_υ, D_υ and H_υ from Eq.(4.1). Fig. 3 illustrates the overall assignment by labeling each P (pink) and R (red) branch of a transition line with its J value. Table 4 provides the comparison of Dunham parameters $T_\upsilon, B_\upsilon, D_\upsilon$ and H_υ for $B_1(^3\sum_u^-)0_u^+(\upsilon' = 10)$ from earlier publications [21] and our study, where the fitting uncertainty (95% C.I.) are given in parentheses.

Table 3
Comparison of obtained transition lines and the Cariou's atlas.

This Work			Cariou [18]			Difference
Line No.	Frequency (GHz)	Gap (GHz)	Line No.	Frequency (GHz)	Gap (GHz)	(GHz)
6	674402.204(62)	–	[1500]	674402.243	–	0.039
12	674411.033(62)	8.829	[1501]	674411.018	8.775	−0.015
13	674414.794(62)	3.761	[1502]	674414.810	3.792	0.016
28	674458.691(62)	43.896	[1506]	674458.712	43.902	0.021
30	674462.546(62)	3.856	[1507]	674462.531	3.819	−0.015
33	674475.016(62)	12.47	[1508]	674475.044	12.513	0.028
35	674480.954(62)	5.938	[1510]	674480.983	5.939	0.029
47	674509.205(62)	28.252	[1513]	674509.182	28.199	−0.023
62	674530.537(62)	21.332	[1515]	674530.527	21.345	−0.010
69	674545.275(62)	14.738	[1517]	674545.241	14.714	−0.034
84	674586.547(62)	41.272	[1521]	674586.534	41.293	−0.013
92	674600.379(62)	13.832	[1523]	674600.346	13.812	−0.033
101	674611.046(62)	3.372	[1525]	674611.021	3.270	−0.025
103	674613.634(62)	2.588	[1526]	674613.621	2.600	−0.013
110	674627.320(62)	13.686	[1527]	674627.321	13.700	0.001
125	674656.200(62)	28.879	[1529]	674656.194	28.873	−0.006
136	674671.480(62)	15.281	[1531]	674671.492	15.298	0.012
137	674674.161(62)	2.681	[1532]	674674.188	2.696	0.027
160	674708.916(62)	34.755	[1534]	674708.949	34.761	0.033
163	674712.713 (62)	3.797	[1535]	674712.735	3.786	0.022
173	674724.128(62)	11.415	[1536]	674724.142	11.407	0.014
176	674732.734(62)	8.606	[1538]	674732.764	8.622	0.030

T_υ and B_υ were found to be in good accordance with previous research, and the higher-order terms were also fitted in this study, with considerably greater precision. The remaining Dunham parameters for $B_1(^3\sum_u^-)0_u^+(\upsilon'=10)$need much broader spectral scanning, since the current scan only extends the spectrum up to J of 40, and higher terms contribute much more significantly as J rises. The rotational and vibrational constants like ω_e and α_e required more data from other $B_1 \leftarrow X_1$ transition lines with different υ' value.

4.4. Frequency locking

Since the frequency of transition lines was determined using the SAS approach, laser frequency locking may be performed in a single resonance line. The signal can be modulated by EOPM, and the dispersion-shaped waveform can be demodulated by the lock-in amplifier and sent as an error signal to the locking P-I servo (Newfocus, LB1005). The frequency of the servo may be regulated by adjusting the voltage of the PZT via the P-I circuit inside the

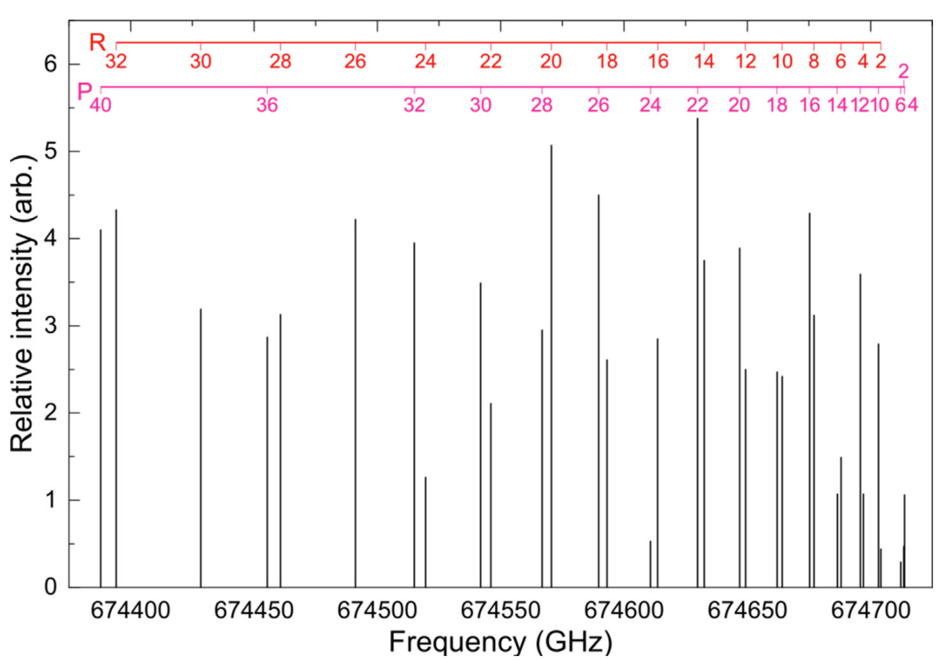

Fig. 3. Line assignment of $B_1\,(^3\Sigma_u^-)0_u^+$ (υ' = 10) ← $X_1(^3\Sigma_g^-)0_g^+$ (υ = 5). Black: experimental results; pink: assigned lines for the P branch; red: assigned lines for the R branch. (Relative frequency and intensity are given with respect to the line 101). (For interpretation of the references to colour in this figure legend, the reader is referred to the web version of this article.)

Table 4
Comparison of Dunham parameters T_υ,B_υ,D_υ and H_υ for $^{130}Te_2$ B_1 $(^3\Sigma_u^-)0_u^+$ (υ' = 10). Numbers in parentheses indicate the fitting uncertainty in the last two digits.

Item	This work (cm^{-1})	Barrow[21] (cm^{-1})
T_υ	23848.93639(65)	23848.96
10^2B_υ	3.10721 (53)	3.1085
10^8D_υ	3.32(98)	
$10^{11}H_\upsilon$	0.35(48)	

servo. The frequency of a Toptica TA-SHG Pro laser can be stabilized with greater than 10 MHz accuracy (10^{-8} $\Delta f/f$) within 90 min, making it feasible to scan the sidebands using EOPM or AOM through modulation when the laser is locked in a certain transition line.

5. Conclusion

To summarize, the molecular $^{130}Te_2$ transition lines were investigated using the SAS technique near 444.4 nm under the uncertainty of 62 MHz, which is necessary for exploring the *e*EDM sensitive transitions of ^{208}PbF molecules in the A $(^2\Sigma^+)$ (υ' = 0) ← $X_1^2\Pi_{1/2}$ (υ = 0) spectroscopic detection. The optical spectrum of Te_2, spanning a frequency range of about 400 GHz, yielded 187 transition lines that are fitted with the Lorentz profile. The molecular transitions of B_1 $(^3\Sigma_u^-)0_u^+$ (υ' = 10) ← $X_1(^3\Sigma_g^-)0_g^+$ (υ = 5) were identified with *J* up to 40, while Dunham parameters T_υ, B_υ, D_υ and H_υ of the B_1 (υ' = 10) state in the Dunham model were updated using the least squares fitting approach. A Toptica TA-SHG Pro laser was then demonstrated to be stabilized in a 10 MHz (10^{-8} $\Delta f/f$) precision by locking to a single Te_2 absorption line through a P-I servo. Our work not only contributes to a detailed frequency reference atlas of Te_2 near 444.4 nm which might be helpful in other spectral experiments, but is also critical to design an *e*EDM measurement using the PbF molecule that is targeted for exploring the fundamental physics beyond the Standard Model.

CRediT authorship contribution statement

Qinning Lin: Conceptualization, Investigation, Software, Writing – original draft, Formal analysis. **Renjun Pang:** Investigation, Methodology. **Zesen Wang:** Investigation, Visualization. **Shunyong Hou:** Supervision. **Hailing Wang:** Supervision, Funding acquisition. **Jianping Yin:** Supervision, Funding acquisition. **Tao Yang:** Writing – review & editing, Supervision, Funding acquisition.

Declaration of Competing Interest

The authors declare that they have no known competing financial interests or personal relationships that could have appeared to influence the work reported in this paper.

Acknowledgement

We thank the support from the National Natural Science Foundation of China (11834003, 11874151, 91536218 and 11674096), the Fundamental Research Funds for the Central Universities, the Program for Professor of Special Appointment (Eastern Scholar) at Shanghai Institutions of Higher Learning, and the Young Top-Notch Talent Support Program of Shanghai. LQN would like to acknowledge the contribution of Prof. John E. Moore Furneaux and Prof. Jiang Yanyi for beneficial discussion and Dr. Zhou Min for the assistant about the frequency locking issue.

Appendix A. Supplementary material

Supplementary data to this article can be found online at https://doi.org/10.1016/j.saa.2021.120754.

References

[1] J.J. Hudson, D.M. Kara, I.J. Smallman, B.E. Sauer, M.R. Tarbutt, E.A. Hinds, Improved measurement of the shape of the electron, Nature 473 (2011) 493–496, https://doi.org/10.1038/nature10104.
[2] W.B. Cairncross, D.N. Gresh, M. Grau, K.C. Cossel, T.S. Roussy, Y. Ni, Y. Zhou, J. Ye, E.A. Cornell, Precision Measurement of the Electron's Electric Dipole Moment Using Trapped Molecular Ions, Phys. Rev. Lett. 119 (2017), https://doi.org/10.1103/PhysRevLett.119.153001 153001.
[3] A. Collaboration, Improved limit on the electric dipole moment of the electron, Nature 562 (2018) 355–360, https://doi.org/10.1038/s41586-018-0599-8.
[4] T.A. Isaev, S. Hoekstra, R. Berger, Laser-cooled RaF as a promising candidate to measure molecular parity violation, Phys. Rev. A 82 (2010), https://doi.org/10.1103/PhysRevA.82.052521 052521.
[5] N.M. Fazil, V.S. Prasannaa, K.V.P. Latha, M. Abe, B.P. Das, RaH as a potential candidate for electron electric-dipole-moment searches, Phys. Rev. A 99 (2019), https://doi.org/10.1103/PhysRevA.99.052502 052502.
[6] P. Aggarwal, V.R. Marshall, H.L. Bethlem, A. Boeschoten, A. Borschevsky, M. Denis, K. Esajas, Y. Hao, S. Hoekstra, K. Jungmann, T.B. Meijknecht, M.C. Mooij, R.G.E. Timmermans, A. Touwen, W. Ubachs, S.M. Vermeulen, L. Willmann, Y. Yin, A. Zapara, Lifetime measurements of the $A^2\Pi_{1/2}$ and $A^2\Pi_{3/2}$ states in BaF, Phys. Rev. A 100 (2019), https://doi.org/10.1103/PhysRevA.100.052503 052503.
[7] Z.H. Yang, J. Li, Q.N. Lin, L. Xu, H.L. Wang, T. Yang, J.P. Yin, Laser-cooled HgF as a promising candidate to measure the electric dipole moment of the electron, Phys. Rev. A 99 (2019), https://doi.org/10.1103/PhysRevA.99.032502 032502.
[8] V.S. Prasannaa, A.C. Vutha, M. Abe, B.P. Das, Mercury monohalides: suitability for electron electric dipole moment searches, Phys. Rev. Lett. 114 (2015), https://doi.org/10.1103/PhysRevLett.114.183001 183001.
[9] M. Denis, P.A.B. Haase, R.G.E. Timmermans, E. Eliav, N.R. Hutzler, A. Borschevsky, Enhancement factor for the electric dipole moment of the electron in the BaOH and YbOH molecules, Phys. Rev. A 99 (2019), https://doi.org/10.1103/PhysRevA.99.042512 042512.
[10] S. Sabor, D. Fadili, A. Touimi Benjelloun, M. Benzakour, M. McHarfi, Computational spectroscopy of diatomic tungsten carbide, WC, I. Mol. Spectrosc., 371 (2020) 111305. 10.1016/j.jms.2020.111305.
[11] V.S. Prasannaa, N. Shitara, A. Sakurai, M. Abe, B.P. Das, Enhanced sensitivity of the electron electric dipole moment from YbOH: The role of theory, Phys. Rev. A 99 (2019), https://doi.org/10.1103/PhysRevA.99.062502 062502.
[12] N.E. Shafer-Ray, Possibility of 0-g-factor paramagnetic molecules for measurement of the electron's electric dipole moment, Phys. Rev. A 73 (2006), https://doi.org/10.1103/PhysRevA.73.034102 034102.
[13] K.I. Baklanov, A.N. Petrov, A.V. Titov, M.G. Kozlov, Progress toward the electron electric-dipole-moment search: Theoretical study of the PbF molecule, Phys. Rev. A 82 (2010), https://doi.org/10.1103/PhysRevA.82.060501 060501.
[14] T. Yang, Spectroscopic and Theoretical Study of Lead Monofluoride Toward Measuring the Permanent Electric Dipole Moment of the Electron, in, Oklahoma University, 2012.
[15] R.J. Mawhorter, B.S. Murphy, A.L. Baum, T.J. Sears, T. Yang, P.M. Rupasinghe, C. P. McRaven, N.E. Shafer-Ray, L.D. Alphei, J.-U. Grabow, Characterization of the ground X_1 state of $^{204}Pb^{19}F$,$^{206}Pb^{19}F$,$^{207}Pb^{19}F$, and $^{208}Pb^{19}F$, Phys. Rev. A 84 (2011), https://doi.org/10.1103/PhysRevA.84.022508 022508.
[16] Y. Makdisi, K.S. Bhatia, Ultraviolet and visible spectra of tellurium I, J PHYS B-AT MOL OPT 15 (1982) 909–913, https://doi.org/10.1088/0022-3700/15/6/016.
[17] J.D. Gillaspy, J. Feinberg, B. Fischer, C.J. Sansonetti, Absolute wavelength determinations in molecular tellurium: new reference lines for precision laser spectroscopy: errata, J. Opt. Soc. Am. B 9 (1992) 2414–2419, https://doi.org/10.1364/josab.9.001401.
[18] J. Cariou, P. Luc, Atlas du Spectre d'Absorption de la Molécule Tellure, Partie 5: 21,100–23,800 cm^{-1} in, CNRS, 1980, pp. 70.
[19] P. Dupre, Very numerous rovibrational levels of tellurium vapor $^{130}Te_2$ induced laser transitions, Opt. Commun. 64 (1987) 431–436, https://doi.org/10.1016/0030-4018(87)90313-0.
[20] J. Vergès, C. Effantin, O. Babaky, J. d'Incan, S.J. Prosser, R.F. Barrow, The Laser Induced Fluorescence Spectrum of Te_2 Studied by Fourier Transform Spectrometry, Phys. Scr. 25 (1982) 338–350, https://doi.org/10.1088/0031-8949/25/2/013.
[21] R. Barrow, R. Du Parcq, Rotational analysis of the $A0_u^+$, $B0_u^+$ – X 0_g^+systems of gaseous Te_2, Proc. R. Soc. London, Ser. A, 327 (1972) 279-287. 10.1098/rspa.1972.0045.
[22] J. Verges, J. d'Incan, C. Effantin, D.J. Greenwood, R.F. Barrow, Laser-excited fluorescence of gaseous Te2studied by Fourier transform spectrometry, J PHYS B-AT MOL OPT 12 (1979) L301–L304, https://doi.org/10.1088/0022-3700/12/10/004.

[23] L.S. Ma, P.h. Courteille, G. Ritter, W. Neuhauser, R. Blatt, Spectroscopy of Te_2 with modulation transfer: Reference lines for precision spectroscopy in Yb^+ at 467 nm, Appl. Phys. B Photophys. Laser Chem. 57 (3) (1993) 159–162, https://doi.org/10.1007/BF00334529.

[24] J.R.M. Barr, J.M. Girkin, A.I. Ferguson, G.P. Barwood, P. Gill, W.R.C. Rowley, R.C. Thompson, Interferometric frequency measurements of $^{130}Te_2$ transitions at 486 nm, Opt. Commun. 54 (1985) 217–221, https://doi.org/10.1016/0030-4018(85)90294-9.

[25] T.J. Scholl, S.J. Rehse, R.A. Holt, S.D. Rosner, Absolute wave-number measurements in $^{130}Te_2$: reference lines spanning the 420.9-464,6-nm region, J. Opt. Soc. Am. B 22 (2005) 1128–1133, https://doi.org/10.1364/josab.22.001128.

[26] J. Coker, H.Q. Fan, C.P. McRaven, P.M. Rupasinghe, T.Z. Yang, N.E. Shafer-Ray, J. E. Furneaux, Cavity dispersion tuning spectroscopy of tellurium near 444.4 nm, J. Opt. Soc. Am. B-Opt. Phys. 28 (2011) 2934–2939, https://doi.org/10.1364/Josab.28.002934.

[27] T. Dutta, D. De Munshi, M. Mukherjee, Absolute Te_2 reference for barium ion at 455.4 nm, J. Opt. Soc. Am. B-Opt. Phys. 33 (2016) 1177–1181, https://doi.org/10.1364/Josab.33.001177.

[28] T. Dutta, M. Mukherjee, High resolution spectroscopy on Te_2: New lines for reference, Spectrochim. Acta A 208 (2019) 109–113, https://doi.org/10.1016/j.saa.2018.09.055.

[29] I.S. Burns, J. Hult, C.F. Kaminski, Use of $^{130}Te_2$ for frequency referencing and active stabilisation of a violet extended cavity diode laser, Spectrochim. Acta A 63 (2005) 905–909, https://doi.org/10.1016/j.saa.2005.10.053.

[30] K. König, P. Imgram, J. Krämer, B. Maaß, K. Mohr, T. Ratajczyk, F. Sommer, W. Nörtershäuser, On the performance of wavelength meters: Part 2—frequency-comb based characterization for more accurate absolute wavelength determinations, Appl. Phys. B 126 (2020) 86, https://doi.org/10.1007/s00340-020-07433-4.

[31] T. Udem, J. Reichert, R. Holzwarth, T.W. Hänsch, Absolute Optical Frequency Measurement of the Cesium D_1 Line with a Mode-Locked Laser, Phys. Rev. Lett. 82 (1999) 3568–3571, https://doi.org/10.1103/PhysRevLett.82.3568.

[32] D.L. Mantia, A Highly Stable and Repeatable Source For Spectroscopy of the BO_u^+ - XO_g^+ Transitions In $^{130}Te_2$, in, Oklahoma University, 2014, pp. 103.

[33] J.L. Dunham, The Energy Levels of a Rotating Vibrator, Phys. Rev. 41 (1932) 721–731, https://doi.org/10.1103/PhysRev.41.721.